Examining Stress Relaxation in a Dissimilar Metal Weld Subjected to Postweld Heat Treatment

Journal Item

Examining stress relaxation in a dissimilar metal weld subjected to post weld heat treatment

K. Abburi Venkata *
C. E. Truman

University of Bristol
Department of Mechanical Engineering
Bristol, BS8 1TR, United Kingdom
Email: k.abburivenkata@bristol.ac.uk

J Araujo de Oliveira
A. N. Forsey
P. J. Bouchard

The Open University
School of Engineering & Innovation
Milton Keynes, MK7 6AA, United Kingdom

A. Achouri
S. Gungor

The Open University
School of Engineering & Innovation
Milton Keynes, MK7 6AA, United Kingdom

S. Khayatzadeh

University of Strathclyde
Advanced Forming Research Centre
Glasgow, G1 1XQ, United Kingdom

ABSTRACT

Dissimilar metal welds are often required in nuclear power plants to join components made from austenitic steels to those from ferritic steels, particularly in fast breeder reactor plants to join the intermediate heat exchanger to the steam generator. The process of welding alters the microstructure of the base materials and also causes residual stresses to form, both due to the change in the microstructure and the differing thermal histories in various regions. Post-weld heat treatment (PWHT) is required to relieve the residual stresses and achieve preferable microstructural gradients across the weld joint. Therefore, in order to arrive at the optimal PWHT process, it is necessary to investigate the effects of heat treatment on the joint integrity, microstructure and residual stress relaxation in the welds.

To investigate this effect of PWHT on the residual stress relaxation and corresponding alteration of microstructure across a welded joint, a dissimilar weld between modified 9Cr-1Mo (P91) steel and austenitic stainless steel AISI 316LN was made using autogenous electron beam (EB) welding. To achieve this, the welding process was first modelled numerically using finite element analysis and the residual stress predictions were validated with experimental investigation using neutron diffraction. The validated model was then used to study the residual stress relaxation through the simulation of PWHT. The predicted stress relaxation was compared with contour method measurement of residual stresses in the actual welded plate subjected to PWHT. The results indicate that albeit some relaxation of residual stresses during PWHT, there is still a significant portion of highly localised residual stresses left in the specimen.

Keywords: Post-weld heat treatment, stress relaxation, residual stress, contour method, finite element analysis

*Address all correspondence to this author.

INTRODUCTION

Welding is one of the most effective and extensively used joining process in many industries, especially in nuclear power plants [1] and is the primary source of residual stresses in components. Residual stresses are usually harmful for the service life of the component by contributing to brittle fracture, corrosive cracking, creep damage and although they are usually accounted for through a safety factor in the design of a pressure vessel, this may not be sufficient for every case [2–5]. Post weld heat treatment (PWHT) is often recommended in the codes and standards for pressure vessles or pipes, in order to achieve the required microstructure and mechanical properties of the joint, in terms of strength and toughness, and relax the residual stresses [6–9]. Modified 9Cr-1Mo (P91) is a creep strength enhanced ferritic/martensitic steel that is increasingly being considered as a suitable material for high temperature applications, such as steam generators and fast breeder reactors [10, 11]. Welding of P91 results in a microstructure of untempered martensite in the weld joint, which is highly unfavourable because of its high hardness [12]. Therefore, it is essential that these welded joints are subjected to PWHT prior to service in order to temper the hard martensitic microstructure [13, 14].

Although the residual stresses are considerably reduced by the heat treatment, it is essential to note that they may not be completely relieved and in some cases are merely redistributed [15–17]. As the primary concern for the structural integrity of pressure vessels used in nuclear power plants is creep, the portion of residual stresses retained in the component, after PWHT, may still pose a threat to structural integrity in service and contribute to creep failure. Additionally, the stress triaxiality arising from the residual stress and applied stress acting together can accelerate the possible degradation of microstructure in terms of void formation and microcracks. In order to understand the influence of these retained residual stresses on the structural integrity of the component in service, it is essential to have an accurate estimation of the magnitude and profile of these retained residual stresses.

Finite element (FE) analysis is increasingly being used as a tool for studying welding processes and PWHT effects of welds in terms of residual stresses, strains and distortions. Razakanaivo and Waeckel [18] developed a viscoplastic based model to simulate the process of welding and PWHT in an industrial context on a French vessel steel. Urevc et. al [19] proposed a viscous-elastic-plastic approach for the numerical simulation of the annealing process with stress relieving in 316L steel and tested the model on a simplied welding and PWHT process. They obtained very good agreement between the predicted residual stress state reduction and data provided from literature. Relaxation during heat treament can be attributed to the significant reduction in the yield strength of a material at elevated temperatures, allowing elastic strains to be released and through creep relaxation. It is therefore reasonable to simulate the heat treatment process using elastic-plastic-creep analysis and predict the stress relaxation [20, 21]. A validated FE model of a PWHT is useful to study the effectiveness of the PWHT parameters such as, holding temperature and time, on stress relaxation for a given specimen size and geometry.

The contour method is a destructive technique that is used to measure cross-sectional residual stress profiles in a welded component [22, 23]. The contour method was developed by M B Prime at Los Alamos National Laboratory [24]. It consists of sectioning the part and measuring the out of plane deformation on the cut surface caused by the stress relaxation. From this, a 2-D map of residual stress acting normal to the cut face can be inferred.

In the current research, a numerical model was developed to simulate the EB welding process between 316LN stainless steel and a ferritic/martensitic P91 steel plates, using the FE code, Abaqus V6.12 [25]. The model was validated by comparing the residual stress predictions in a dissimilar metal welded plate with those obtained from an EB welded plate measured using neutron diffraction [26]. The valiated model was utilised to simulate the PWHT process and predict the residual stress relaxation and redistribution subsequent to the heat treatment process. The predicted residual stresses in the welded plate after PWHT were validated through a contour method residual stress measurement on the actual welded plate after PWHT.

SAMPLE

A dissimilar metal weld was produced using EB welding between AISI 316LN austenitic stainless steel and a ferritic/martensitic P91 steel. The chemical composition of the base materials is shown in Table 2. The resulting welded plate was 11 mm thick and measured 250 mm $\times$ 156 mm and a schematic of the welded plate is shown in Figure 1(a). The plates were welded together using a full penetration welding pass, followed by a cosmetic pass using a defocussed beam, which resulted in a depth of penetration of $\sim$ 4.5 mm. Prior to the welding, there was preheating on the P91 side to $\sim$ 150 °C to facilitate the welding process and compensate the difference in the thermo-physical properties of both the materials. The details of the welding process are explained in detail elsewhere [26] and the welding parameters are shown in Table 1.

The weld fusion zone and heat affected zone (HAZ) were $\sim$ 1.1 mm and $\sim$ 0.7 mm wide respectively. A macrograph of the welded plate at the mid-point cross-section is shown in Figure 1(b). Electron backscattering diffraction (EBSD) analysis conducted on as-welded

specimens from the weld fusion zone, HAZ and base material regions indicated that the weld fusion zone is fully martensite/ferrite in the region away from the cosmetic pass (more than 4.5 mm deep) with increased quantities of austenite (13 %) in the region under the influence of cosmetic pass [27].

The plate was subjtected to PWHT after welding in order to relax the residual stresses and achieve the required microstructure by heat treating the plate at 760 °C for 3 h as recommended by the ASME standard for pressure vessels [28] for P91 steel.

Table 1. **Welding parameters**

Pass	Voltage (kV)	Current (mA)	Speed ($m\,min^{-1}$)
Weld pass	125	48	0.5
Cosmetic pass	100	26	0.5

FINITE ELEMENT ANALYSIS

A FE model was developed using Abaqus 6.12 code [25] to simulate the EB welding process between the dissimilar P91 and 316LN plates. The welding process was simulated using sequentially coupled thermo-mechanical analyses. The thermal transients arising from the welding thermal cycle were simulated using block-dumped approach with radiation as the boundary condition. The predicted transient temperature distribution was then provided as input to the mechanical analysis to predict the residual stresses. As P91 steel exhibits solid-state phase transformation (SSPT), the associated volume change due to martensitic phase transformation during the rapid cooling of the weld pool and the corresponding change in the yield strength was modelled in the mechanical analysis using UEXPAN and UHARD subroutines respectively. Temperature dependent thermo-mechanical properties and stress-strain material response were employed in the analysis, the details of which can be found in [29]. The thermo-physical properties of the P91 base material with temperature are shown in Table. 3. The temperature-dependent monotonic strain-strain response of P91 material is shown in Table. 4. For 316LN base material, a temperature dependent cyclic stress-strain response was described using Chaboche parameters shown in Table. 5. The temperature-dependent physical properties of the 316LN base material employed in the analysis are given in Table. 6. The predicted weld fusion boundary using the 1500 °C isotherm was validated by comparing with the cross-sectional weld macrograph and the residual stresses predicted in the plate were validated by measurements using neutron diffraction. These are described in detail and presented in [26, 27, 29]. The predicted residual stress across the weld at mid-thickness of the specimen and its comparison with the measured residual stress in welded plate in the AW condition is shown in Fig. 2. It is noted that a very good agreement is achieved between the predicted and measured residual stresses in the welded plate.

Later FE simulation of the heat treatment process was conducted on the validated weld model using Abaqus v6.14 code [25], in order to study the effects of PWHT on the plate, in terms of residual stress relaxation and redistribution. The simulation was again conducted using sequentially coupled thermal and mechanical analyses to capture the effects of PWHT. During the thermal analysis, the transient thermal distribution in the welded plate was predicted which was then supplied as the input temperature distribution for the mechanical analysis. The welding residual stresses were supplied as the initial state using *Map solution keyword in Abaqus. The thermal analysis was performed using prescribed temperature in Abaqus with a simple tabular distribution of the required temperature

Table 2. **Chemical composition of the base metals in % wt. (Balance Fe) [26]**

Steel	C Nb	Mn Ti	Zr V	Si	P	S	Cr	Mo	Ni	Cu	Al	N
P91	0.11 0.07	0.39 0.004	0.005 0.2	0.27	0.017	$\ll 0.003$	8.82	0.82	0.21	0.17	0.02	0.0464
316LN	0.03 0.005	1.72 0.005	- 0.051	0.39	0.025	$\ll 0.003$	17.5	2.58	11.9	0.195	0.001	0.087

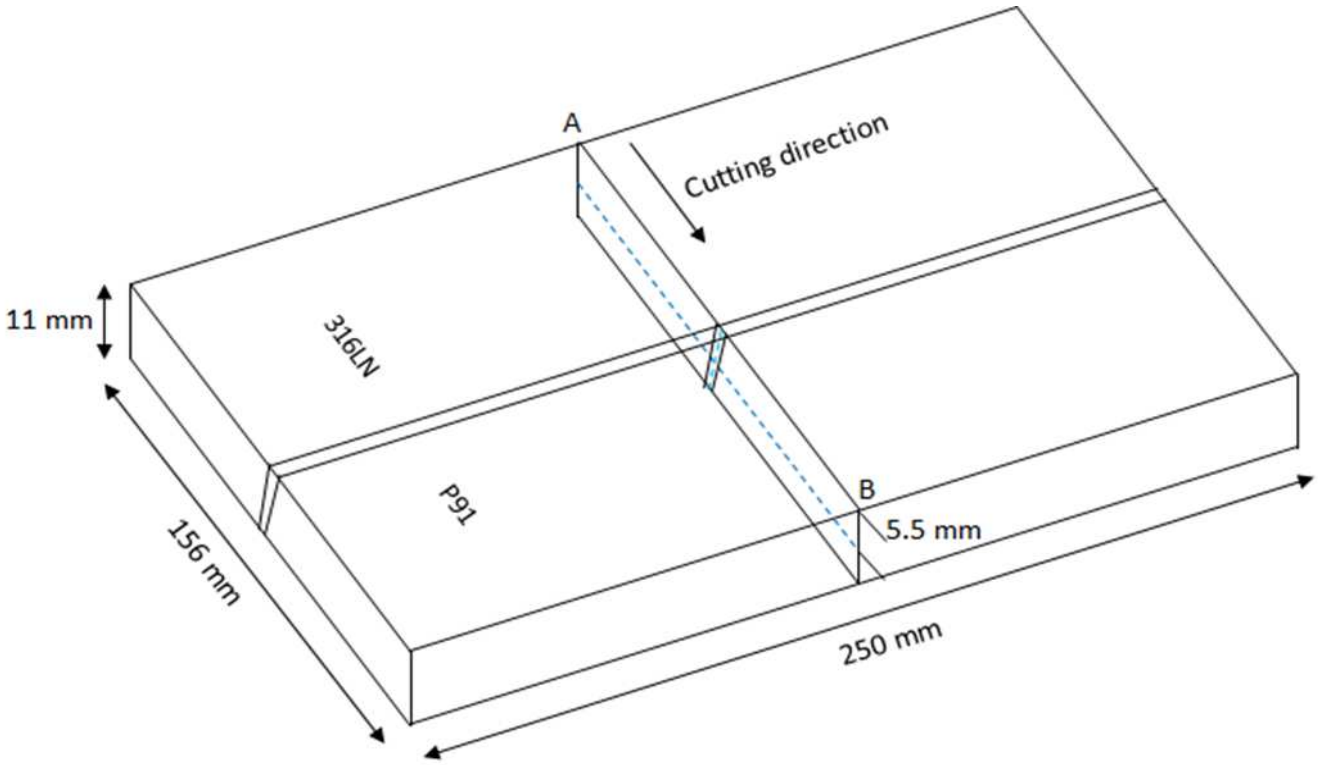

(a) Schematic representation of the welded plate

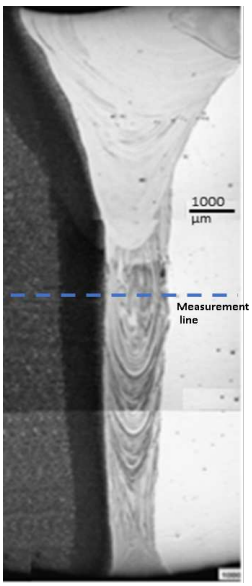

(b) Cross-sectional macrograph of the welded plate

Figure 1. Schematic representation and cross-sectional weld macrograph of the dissimilar metal EB welded specimen

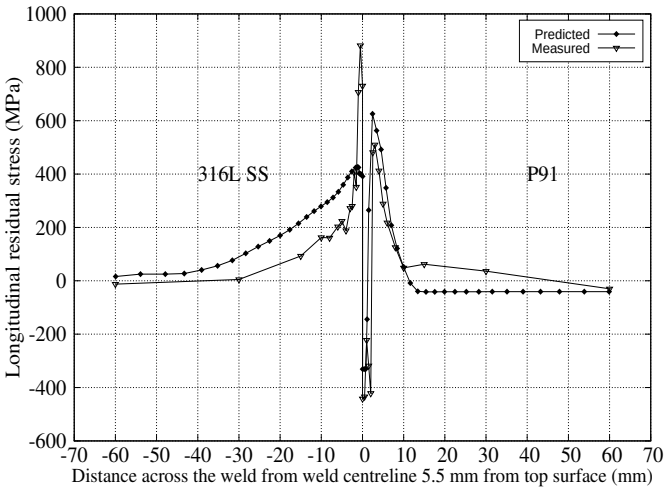

Figure 2. Comparison of predicted and measured residual stresses in the dissimilar welded plate in AW condition across the weld at mid-thickness of the plate [26]

field on the specimen plate. The temperature distribution employed during the PWHT simulation is shown in Figure 3. For the sake of simulation, a heating time of 1 h was employed to heat the specimen to the required temperature (760 °C). Up on reaching this temperature, the specimen is held at this temperature for a duration of 3 h, followed by cooling to room temperature over a period of 8 h. The temperature was chosen as 760 °C in order to achieve maximum relaxation without altering the microstructure, as 760 °C is lower than the austenite start temperature ($AC1$). The FE mesh used in the analysis is shown in Figure 4. The model was meshed using linear hexahedral elements with reduced integration and a mesh size of 1.25 mm × 0.5 mm × 0.7 mm in the weld region, as shown in Figure 4.

The residual stress relaxation was simulated through the reduction of yield strength with temperature during the heating stage and creep relaxation during the holding stage. The holding temperature was set to 760 °C for a duration of 3 h. The creep properties for the weld metal were generated from cross-weld creep tests conducted on PWHT specimens at 650 °C at various stresses ranging from 80 - 120 MPa and extrapolated to the holding temperature (760 °C) using Arrhenius equation for creep as given in Eq.1 [32]. The Norton power law definition for creep can be represented as Eq.2 [33]. By equating Eq.1 and Eq.2, the value of A can be extrapolated at the required temperature from the value at a known temperature. The extrapolation was conducted assuming the stress exponent 'n' did not change with temperature [29, 30]. The creep constants for the materials at 650 °C are given in Table 7. The temperature dependent material properties and stress-strain response for base materials were taken from literature [29, 30, 34] and shown in Table 3 to 6.

$$\dot{\varepsilon} = A^{'} \sigma^{n} e^{(\frac{-Q}{RT})} \tag{1}$$

where $\dot{\varepsilon}$ is the creep strain rate, $A^{'}$ and n are the material constants, Q is the activation energy, T is the temperature, σ is the stress and R is the universal gas constant.

$$\dot{\varepsilon} = A\sigma^{n} \tag{2}$$

where A and n are material constants.

RESIDUAL STRESS MEASUREMENT USING CONTOUR METHOD

The contour method for residual stress measurement is a destructive technique, which is used to calculate a 2D map of the out of plane residual stress along a cut surface. Cutting the component is the most critical step in the contour measurement procedure as all

the succeeding steps depend on the quality of the cut faces created. Commercial wire electro discharge machining (EDM) machines are optimised for conventional applications involving a rough cut followed by several finishing skim cuts to produce a suitable surface finish. However, for the contour method, EDM cutting conditions must be selected for a single cut that produces the surface finish with lowest roughness while minimising cutting artefacts [35]. For the welded plate considered here, the cutting parameters were chosen based on previous experience of cutting ferritic and austenitic materials of similar thickness.

EDM wire entry and exit from the test specimen can introduce cutting artefacts that affect near-surface measurements [35]. Figure 1(a) shows the position of the cut in the welded plate, where the wire entry (A) refers to the end of the specimen that the cut starts where the running wire enters the test specimen and similarly wire exit (B) relates where the running wire leaves the test specimen. To mitigate wire entry and exit cutting artefacts, sacrificial layers [35] were bonded to the outer surface of the plate to create a uniform cross-section and help avoid cutting artefacts. The plate was rigidly clamped in an Agie Charmilles wire EDM machine (CUT 1000) and the contour cut was performed. Note that prior to cutting, the specimens and clamping fixtures were left immersed to reach thermal equilibrium within the EDM deionised water tank.

Prior to making this cut for the contour method, the plate had undergone two prior full width cuts at 156 mm and 81 mm from the reference edge. Both cuts were intended for contour measurement, but this was not possible due to equipment malfunctions. The contour cut presented here was then carried out from the 316LN side of the specimen at a position of 116 mm, which is located in the central section of the three pieces. This cut direction is the opposite of that required to reduce the stress-intensity factor (SIF) during the cut and so some plasticity may have been induced at the weld line as a result. Plasticity during the cut means that somre residual stress has been relieved by inducing plastic deformation and so this relieved stress does not cause a change in cut surface displacement. Due to

Table 3. Thermo-physical properties of P91 steel [29, 30]

Temperature (°C)	Thermal Conductivity $W\,m^{-1}\,°C^{-1}$	Specific heat $J\,kg^{-1}\,°C^{-1}$	Young's Modulus GPa	Poisson's ratio	Density $kg\,m^{-3}$	Thermal expansion $°C^{-1}$
20	26.0359	430.766	218	0.3	7770	1.04e-5
50	26.0359	450.492	216			1.08e-5
100	27.0147	460.538	213			1.1e-5
150	26.8189	470.563	210			1.11e-5
200	28.0914	500.152	208			1.14e-5
250	27.9935	510.188	205			1.15e-5
300	27.8956	520.223	200			1.17e-5
340	29.0701	540.035	195			1.19e-5
375	28.9723	559.751	193			1.18e-5
400	29.168	589.233	191			1.22e-5
450	29.0701	618.866	186			1.26e-5
500	30.0489	638.668	181			1.25e-5
550	30.0489	687.865	176			1.26e-5
600	30.0489	756.607	168			1.26e-5
650	30.0489	854.712	162			1.29e-5
700	30.7341	933.252	153			1.31e-5
750	30.93	1041.18	145			1.31e-5
800	31.0277	923.97	134			1.32e-5
850	29.4617	845.924	125			1.26e-5
900	28.0914	709.152	116			1.34e-5
1000	27.8956	670.484	94			1.36e-5
1100	27.9935	690.544	73.4			1.42e-5
1200	28.0914	691.028	50.9			1.5e-5
1300	28.385	720.886	31.3			1.52e-5
1400	29.2659	721.228	9.79			1.57e-5
1500	29.4617	741.441	9.79			1.61e-5

Table 4. Monotonic stress-strain behaviour of P91 base material at various temperatures [29, 30]

Plastic Strain (%)	0	2	4	5	10	15	20
Temperature (°C)	Stress (MPa)						
23	507	585	655	666	675	644	537
200	456	471	588	586	511	428	360
400	432	476	533	544	516	410	200
550	350	400	416	409	385	341	270
650	257	266	272	251	225	203	179
850	75.2	84.8	91.73	94.61	97.5	98.36	97.8
1000*	50						
1200*	30						
1500*	2						

*Data were extrapolated for temperatures marked with an asterisk.

Table 5. Chaboche parameters for mixed hardening for 316L stainless steel [31]

Temperature (°C)	$\sigma\|_0$ (MPa)	C_1 (MPa)	γ_1	C_2 (MPa)	γ_2	Q_{inf} (MPa)	b
20	125.6	156,435.00	1410.85	6134	47.19	153.4	6.9
275	97.6	100,631.00	1410.85	5568	47.19	154.7	6.9
550	90.9	64,341.00	1410.85	5227	47.19	150.6	6.9
750	71.4	56,232.00	1410.85	4108	47.19	57.9	6.9
900	66.2	0.05	1410.85	292	47.19	0	6.9
1000	31.82	0	1410.85	0	47.19	0	6.9
1100	19.73	0	1410.85	0	47.19	0	6.9
1400	2.1	0	1410.85	0	47.19	0	6.9

this processing route, some relaxation of the residual stress from the as received sample is inevitable.

Following the contour cut, the cut parts were cleaned, dried and left in a temperature-controlled laboratory to reach thermal equilibrium before starting surface profile measurements. The topography of the opposing cut surfaces was measured using a Zeiss Eclipse co-ordinate measuring machine (CMM), fitted with a Micro- Epsilon laser probe and a 3 mm diameter ruby-tipped Renishaw PH10M touch trigger probe. The laser sensor was used to scan the surface with a point spacing of 0.05 mm in both x and y directions, but the perimeters of the cut parts were measured with the touch probe. The perimeter data was used to define the geometry of the surfaces for the data processing step.

The data sets for opposing cut surfaces were aligned using the measured perimeters and then interpolated onto a common grid before averaging to remove errors due to shear stress and possible anti-symmetric cutting artefacts [36]. Noise in the displacement data is unavoidable due to the roughness of the EDM cut surfaces and uncertainty in CMM measurements. Since the stress calculation magnifies the noise in the data, it is important to smooth the surface displacements [24]. For this plate, data smoothing was conducted using a StressMap proprietary algorithm called Enhanced Polyfit. The smoothing was biased in the through-thickness direction, since significant stress gradients were not expected along the y axis. However, the level of smoothing had to be kept to a minimum along the x axis in order to capture the steep stress gradients expected in this specimen. The level of smoothing was sequentially increased until the plot of residuals started to show a bias in the weld region, *i.e.* the sharp stress variation started being oversmoothed. The smoothing level selected for the measurement was a value just lower than that which showed bias. Note that this method of selection was used because global measures of smoothing optimisation [36–38] were found unsuitable for this particular stress profile, as they lead to oversmoothed data at the sharp residual stress variation in the region of interest.

A 3-dimensional finite element model based on the measured perimeter of one of the cut parts was built using Abaqus v6.13 code. The model was meshed using linear hexahedral elements with reduced integration (C3D8R) and a global mesh size of 1 mm and refined

Table 6. Physical and mechanical properties for the Type 316H stainless steel [29, 31]

Temperature °C	Specific Heat kJ kg^{-1} °C^{-1}	Conductivity W m^{-1} °C^{-1}	Density kg m^{-3}	Poisson's ratio	Thermal Expansion $\times 10^6$ mm mm^{-1} °C^{-1}	Young's Modulus GPa
20	0.488	14.12	7966	0.294	14.56	195.6
100	0.502	15.26			15.39	191.2
200	0.520	16.69			16.21	185.7
300	0.537	18.11			16.86	179.6
400	0.555	19.54			17.37	172.6
500	0.572	20.96			17.78	164.5
600	0.589	22.38			18.12	155.0
700	0.589	23.81			18.43	144.1
800	0.589	25.23			18.72	131.4
900	0.589	26.66			18.99	116.8
1000	0.589	28.08			19.27	100.0
1100	0.589	29.50			19.53	80.0
1200	0.589	30.93			19.79	57.0
1300	0.589	32.35			20.02	30.0
1400	0.589	33.78			20.21	2.0

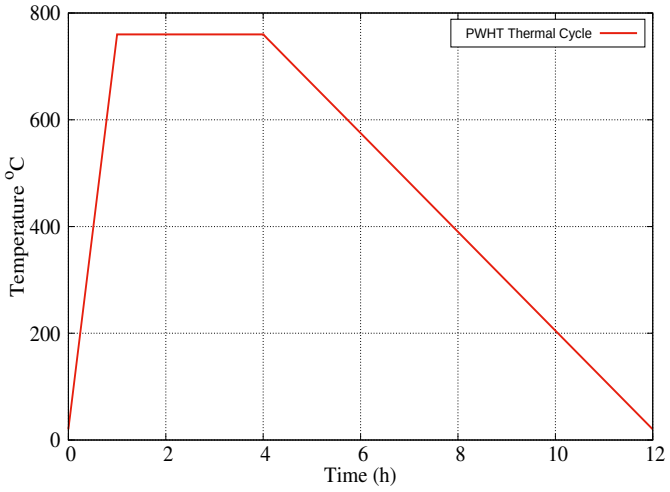

Figure 3. Thermal cycle used in the PWHT simulation

to 0.2 mm in the weld region, as shown in Figure 5. The mesh size increased linearly at a distance of 5 mm away from the cut face to reduce computation time. The room temperature Youngs moduli of P91 and 316LN used in the model were 197.5 and 218 GPa respectively and Poisson's ratios were taken as 0.27 and 0.3 [26, 29]. Homogeneous isotropic elastic properties were assumed within each weld region, with values taken as equal to that in the respective parent material. The smoothed displacements were reversed and applied as boundary conditions at the cut surface nodes. Additional constraints were imposed to prevent rigid body motion of the model. Finally, the residual stress component acting normal to the cut faces was calculated using a linear elastic stress analysis.

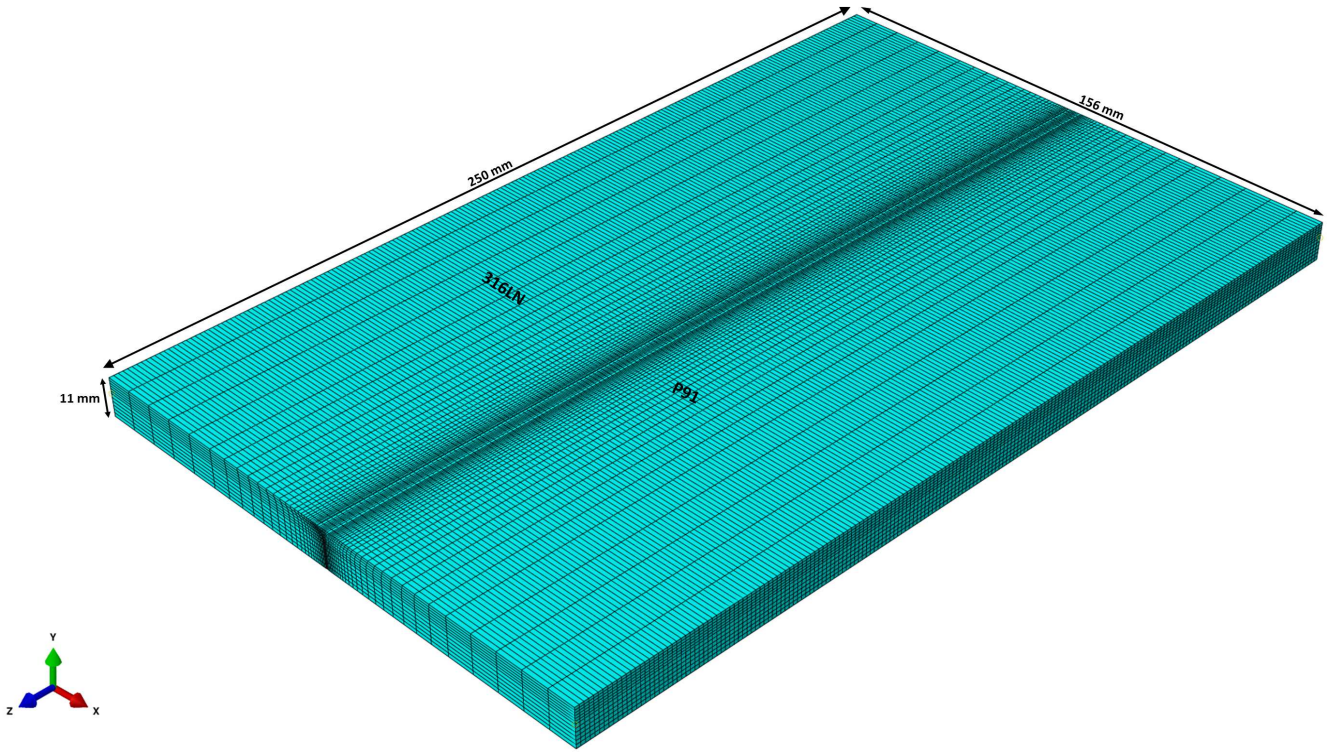

Figure 4. Finite element mesh in PWHT simulation

Table 7. Creep constants used in PWHT simulation

Material	A in (MPa, hour)	n
P91	1E-29	12.6
Weld	7E-24	9.18
316LN	1.60E-27	7.3

RESULTS

Figure 6 shows the contour plot of the predicted retained residual stress across the weld after PWHT from the simulation. This can be directly compared with the contour plot produced using contour method in Figure 7, which shows the longitudinal residual stress found experimentally. The predicted residual stress in longitudinal direction is shown in Figure 8. This is a line plot extracted from the centre of the plate, across the weld, at mid-thickness of the specimen and displays the retained residual stresses in the weld longitudinal, transverse and normal directions following the PWHT. This shows that the highest retained residual stress is found in the longitudinal direction and this is the plane in which the contour cut was made. Thus simulation results can be compared with corresponding experimental data from the contour method.

To aid the comparison of the residual stress profile across the PWHT weld from predictions and measurements, contour method and simulation mid-thickness line plots are overlaid in Figure 9. As the contour method is a destructive technique it cannot be performed on the same weld in AW condition. Instead a non-destructive residual stress measurement technique was used, specifically neutron diffraction. A line plot of the experimental AW and PWHT longitudinal residual stress, at mid-thickness can be seen in Figure 10. Hardness values across the weld before and after PWHT are shown in Figure 11. This shows that although PWHT reduced the hardness

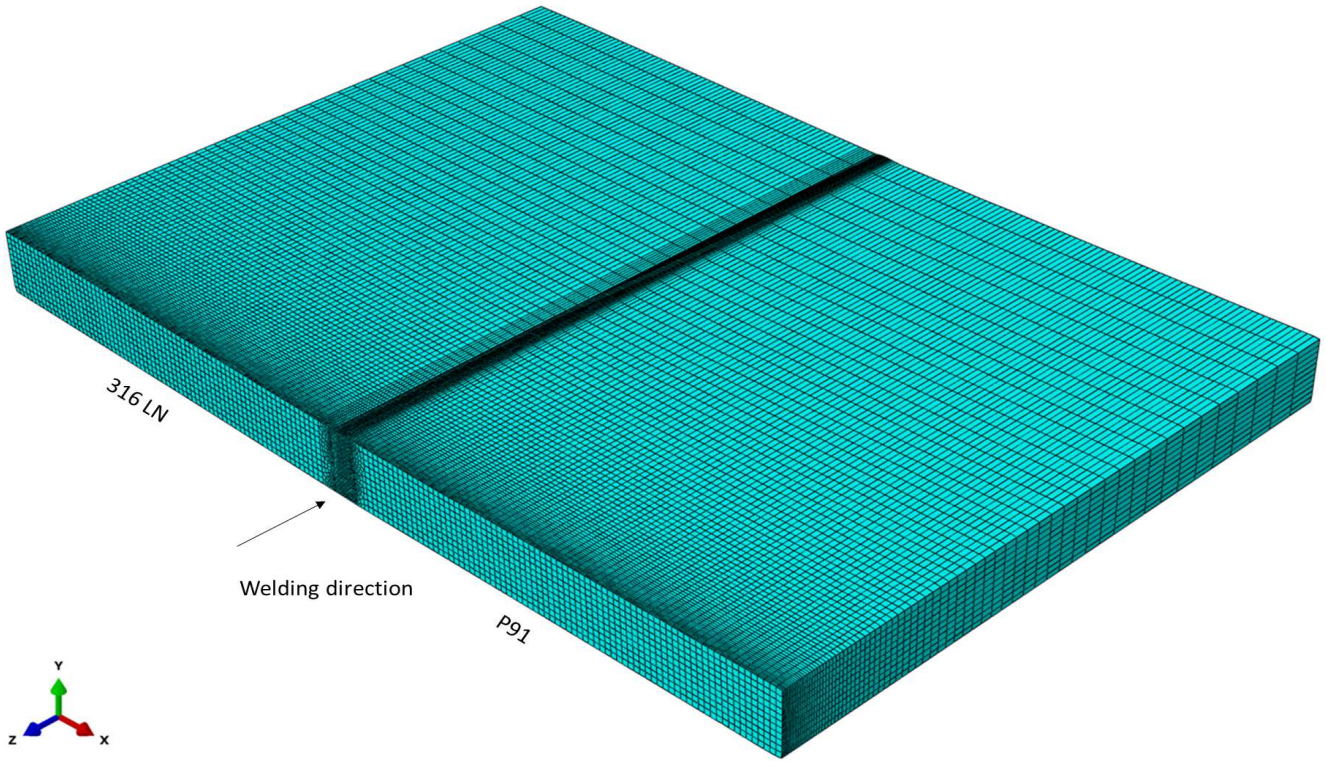

Figure 5. Finite element mesh used for contour measurement

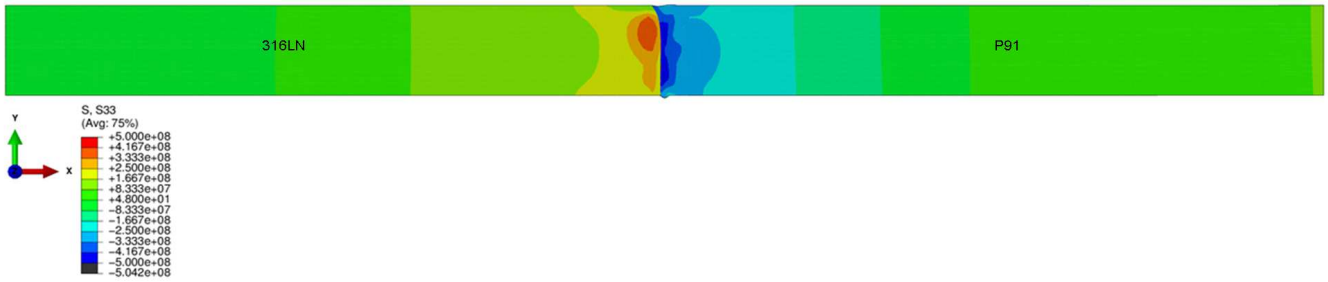

Figure 6. Predicted contour of the longitudinal residual stress across the weld in the welded plate

in the weld and HAZ region on P91 side, the hardness is still considerably higher compared to the base materials.

Figure 12(a) indicates the predicted elastic strain relaxation at a point in the weld fusion zone during the PWHT thermal cycle. The relaxation of the plastic strain at the same point during the PWHT cycle is illustrated in Figure 12(b). The creep strain accumulated during the simulation is shown in Figure 12(c). From the graph, it can be seen that the creep strain accumulates during the holding stage where a portion of the elastic strain is converted to creep strain.

DISCUSSION

Looking at Figure 12(b), it is evident that the plastic strain has relaxed significantly during the heating stage and has not changed during the holding and cooling stages. As the specimen is heated, the plastic strain is relaxed based on the reduction of the yield strength of the material with increasing temperature. After this, the plastic strain remains unchanged throughout the holding and cooling stages.

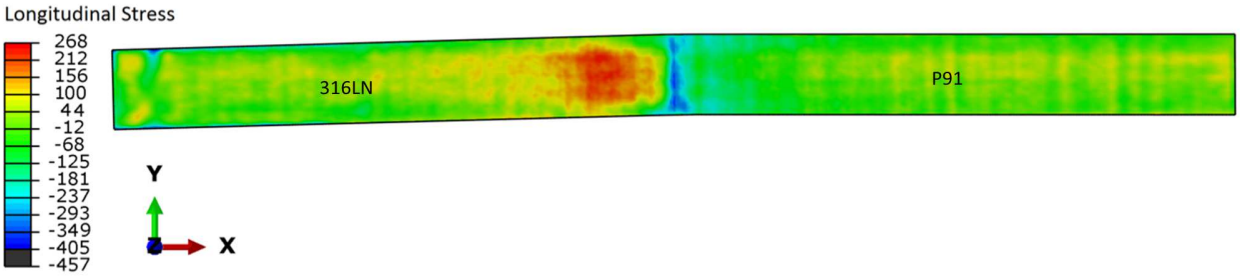

Figure 7. Measured contour plot of the longitudinal residual stress across weld in the welded plate

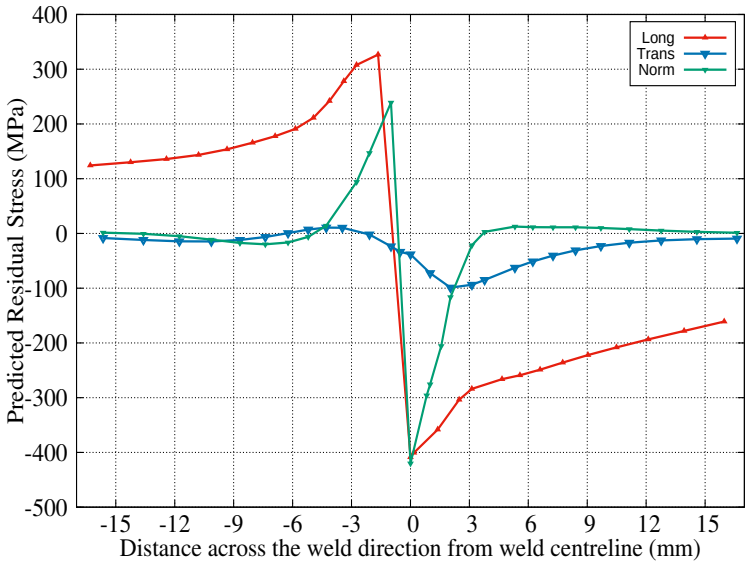

Figure 8. Predicted residual stress across the weld at mid-thickness of the welded plate

From the residual stress profiles in Figures 6 and 7, it can be seen that the weld centre is predominantly under compression, however the region on 316LN side indicates the presence of a highly stressed region in tension. The compressive stress state exists throughout the thickness of the specimen, which can be explained from solid-state martensitic phase transformation during rapid cooling of the welded plate after welding process.

The comparison of the line plot of longitudinal residual stress across the weld at mid-thickness from simulation and measurement is shown in Figure 9. From Figure 9, it can be seen that the stress profile on 316LN side has a good agreement between the predictions and measurements, but the peak stress location differs from the simulation and measurement. There is, however, little morphological similarity between the 2D residual stress contour plots from the simulation (Figure 6) and experimental (Figure 7). However, despite the local distributions differing, the values in each region are very similar. This can be seen more clearly in the comparative line plot in Figure 9, but here, there is a clear difference in peak stress position.

It is unclear if this apparent difference is due to release of plasticity during the contour cut, as the cutting direction was carried out from 316LN side and is opposite of that required to reduce SIF. Comparing the profiles on P91 side, there is a consistent difference of $\sim$100 MPa between the predicted and measured values. This variation disappears at about 40 mm away from the fusion zone, where the stress profiles start to match very well. This variation can be attributed to various reasons such as lack of characteristic material properties, in particular those related to creep, for the base material and the various regions of the weld and HAZ regions on P91 side and the use of extrapolation scheme to generate creep constants at the required temperature.

The hardness map in Figure 11 shows that after PWHT the hardness is reduced and that the transition between parent and HAZ is more gradual. This is consistent with the redistribution of residual stress predicted by the model in Figure 13, where the residual stresses

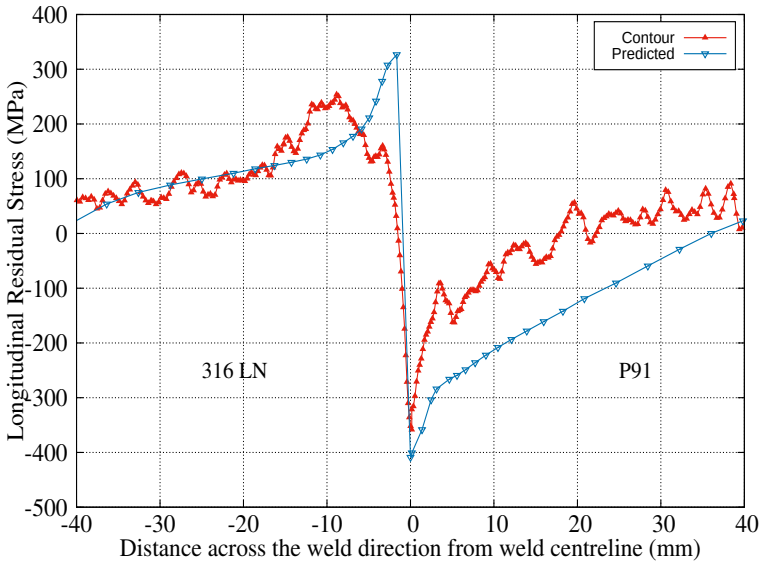

Figure 9. Contour plot indicating longitudinal residual stress profile across weld in the welded plate

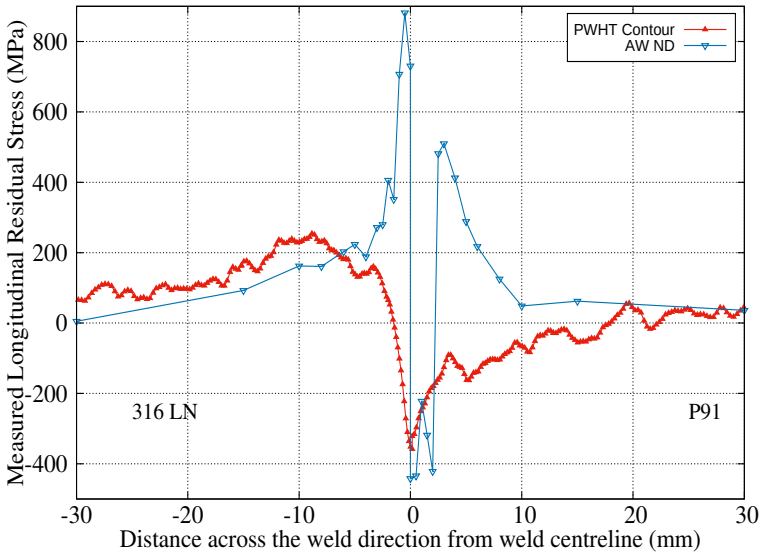

Figure 10. Comparison of the measured residual stress plot across the weld in AW and PWHT condition

at the interface are both lower and more gradual in the PWHT than in the AW condition.

Figure 13 shows the simulated values which relate to the experimental measurements of longitudinal residual stress shown in Figure 10. The model predicts very similar features in the residual stress profile, but the position and magnitude of the peaks varies predominantly in the 316LN HAZ region for both measurements.

The residual stress profile after relaxation for both the simulation in Figure 8, and the experimental in Figure 9, imply that there is significant amount of stress retained in the specimen (~ -400 MPa in longitudinal and normal direction) even after PWHT. The stress profile indicates that the stresses at the weld centre are predominantly compressive in nature and the tensile stresses are observed on the 316LN side. The compressive residual stresses may be explained by SSPT experienced by P91 steel during rapid cooling after welding [26].

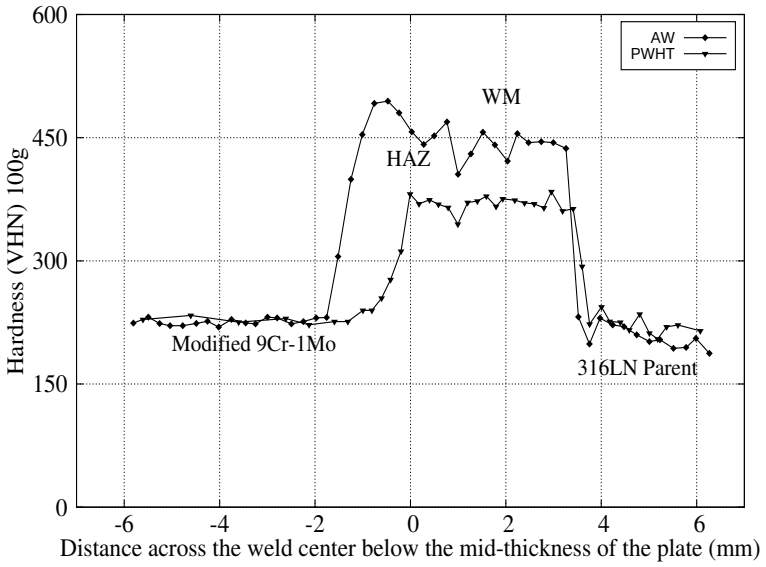

Figure 11. Measured hardness across weld at 1.5 mm below the top surface, before and after PWHT

Figure 12(a) shows the elastic strain increases during the heating of the specimen for the first 1 h. During the holding stage (1 hour to 4 hour), the elastic strain dropped indicating relaxation experienced. Subsequently, the elastic strains dropped further during the cooling of the specimen. A close comparison of Figures 12(a) and 12(c) confirms the same. The creep strain is accumulated until the end of the holding stage after which there is no further strain accumulation.

It is evident from Figure 13, that although heat treatment has relaxed and redistributed the stresses, there is still a significant portion of stress retained especially in the centre of the weld. It is interesting as well that the amount of relaxation observed on the P91 side is significantly higher than that of 316LN side. It should also be noted that for the scope of the paper, the residual stress relaxation during PWHT is alone considered. Therefore, the results are analysed at a particular set of hold time and temperature. Future work will include sensitivity analyses to understand the influence of PWHT parameters such as hold time and temperature on the extent of residual stress relaxation in a dissimilar metal EB weld.

CONCLUSIONS

Based on the finite element simulations and contour measurements conducted on a dissimilar metal welded plate subjected to PWHT, it can be concluded that,

1. Although post-weld heat treatment has reduced the residual stress magnitude and hardness compared to the as-welded condition, significant portion of highly localised residual stress is still retained in the specimen. The extent of the retained stress after PWHT should be determined accurately in order to make reliable structural integrity assessments.
2. The residual stresses in the weld centre in AW condition, were compressive in nature, which can be explained as a result of solid-state phase transformation undergone by P91 steel during rapid cooling after welding process. The residual stress state in the centre of the weld subsequent to PWHT is therefore compressive.
3. The measured and the predicted residual stresses in the welded plate after PWHT agree well, indicating tensile stresses in 316LN side and compressive stresses in P91 side of the welded plate.
4. Microstructure specific accurate material creep properties, at the treatment temperature, are essential to predict the extent of residual stress relaxation reliably during PWHT.

REFERENCES

[1] R.H. Legatt. Residual stresses in welded structures. *International Journal of Pressure Vessels and Piping*, 2008, **85**, pp. 144 - 151.

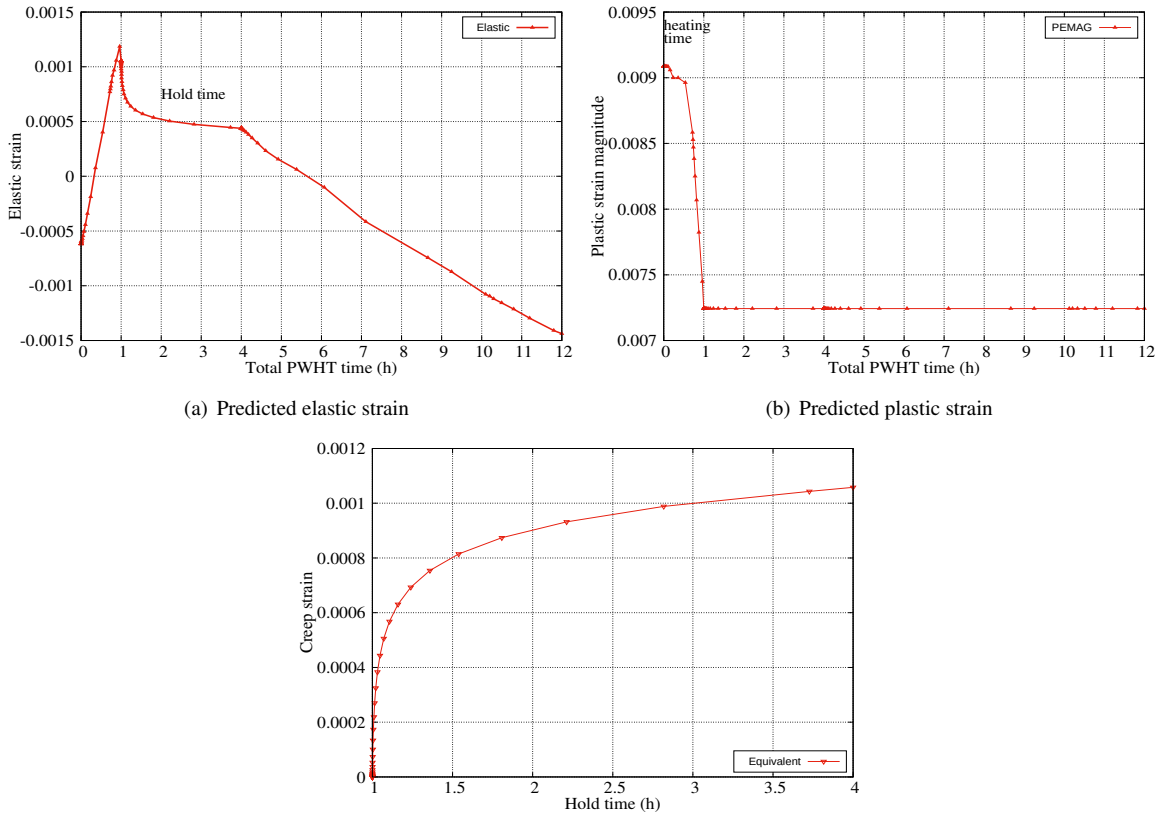

(a) Predicted elastic strain

(b) Predicted plastic strain

(c) Predicted creep strain

Figure 12. Predicted strain in the weld fusion zone of the welded plate

[2] O. Kwon, B. Pathiraj, KM. Nikbin. Effects of residual stress in creep crack growth analysis of cold bent tubes under internal pressure. *International Journal of Pressure Vessels and Piping*, 2001, **78**, pp. 343 - 350.

[3] S. Hossain, C.E. Truman, D.J. Smith, R.L. Peng U. Stuhr. A study of the generation and creep relaxation of triaxial residual stresses in stainless steel. *International Journal of Solids and Structures*, 2007, **44**, pp. 3004 - 3020.

[4] R. C. Wimpory, F. R. Biglari, R. Schneider, K. M. Nikbin, N.P. O'Dowd. Effect of residual stress on high temperature deformation in a weld stainless steel. *Materials Science Forum*, 2006, **524-525**, pp. 311 - 316.

[5] K. M. Nikbin N. P. O'Dowd and F. R. Biglari. Creep crack initiation in a weld steel: effects of residual stress. In *Proceedings of ASME Pressure Vessels and Piping Division Conference*, 2005.

[6] M.C. Zondi. Factors that affect welding-induced residual stress and distortions in pressure vessel steels and their mitigation techniques: A review. *Journal of Pressure Vessel Technology*, 2014, **136**, pp. 040801-1 - 040801-9.

[7] Post weld heat treatment of welded structures; welding technology institute of australia.

[8] K. Ahmed, J. Krishnan. Post-weld heat treatment - case studies. Technical report, Bhabha Atomic Research Centre, 2002.

[9] R. Scott Funderburk. Key concepts in welding engineering: Postweld heat treatment. *Welding Innovation*, 1998, **XV, 2**.

[10] W.F. Newell Jr. Welding and post weld heat treatment of p91 steels. *Welding Journal*, 2010 April, pp. 33 - 36.

[11] M. Sireesha, S. Sundaresan, S.K. Albert. Microstructure and mechanical properties of weld fusion zones in modified 9cr-1mo steel. *Journal of Materials Engineering and Performance*, 2001, **10(3)**, pp. 320 - 330.

[12] S. Sulaiman, D. Dunne. Microstructural and hardness investigations on simulated heat affected zone (haz) in p91 creep resisting steel. *Solid State Science and Technology*, 2007, **15(1)**, pp. 102 - 107.

[13] G. Taniguchi, K. Yamashita. Effects of post weld heat treatment (pwht) temperature on mechanical properties of weld metals for high-cr-ferritic heat-resistant steel. Technical report, Kobelco Technology, 2013, **32**, pp. 33 - 39.

[14] A. Shilbi, F. Starr. Some aspects of plant and research experience in the use of new high strength martensitic steel p91. *International*

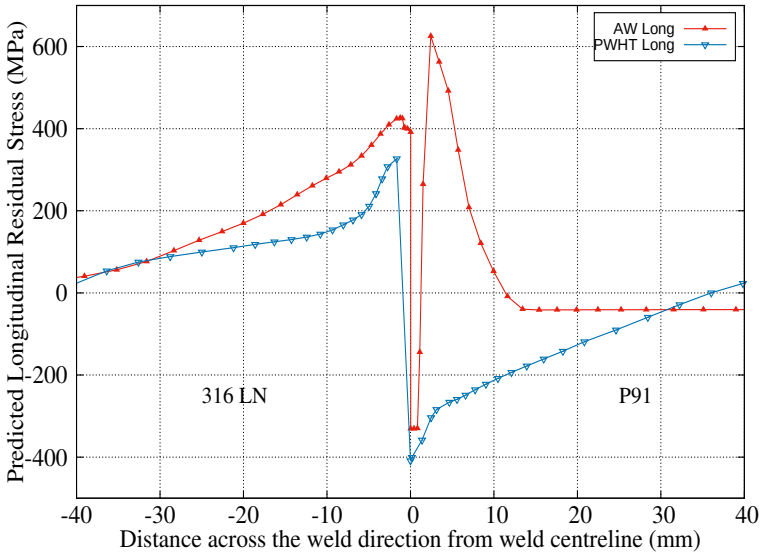

Figure 13. Predicted residual stress across the weld at mid-thickness of the welded plate

Journal of Pressure Vessels and Piping, 2007, **84**, pp. 114 - 122.

[15] P. Xie, H. Zhao, B. Wu S. Gong. Evaluation of residual stresses relaxation by post weld heat treatment using contour method and x-ray diffraction method. *Experimental Mechanics*, 2015, **55(7)**, pp. 1329 - 1337.

[16] Z. Feng. *Processes and mechanisms of welding residual stress and distortion*. CRC Press, 2005.

[17] T.C. Chuvas, P.S.P. Garcia, J.M.Pardal M.P.C. Fonseca. Influence of heat treatment in residual stresses generated in p91 steel-pipe weld. *Materials Research*, 2015, **18(3)**, pp. 614 - 621.

[18] A. Razakanaivo and F. Waeckel. A viscoplastic model for numerical simulation of welding and post-weld heat treatment. *Journal of Physics IV France*, 1999, **9**.

[19] J. Urevc, P. Koc, B. Stok. Numerical simulation of stress relieving of an austenite stainless steel. *Journal of Mechanical Engineering*, 2009, **55(10)**, pp. 590 - 598.

[20] P. Dong, S. Song, J. Zhang. Analysis of residual stress relief mechanisms in post-weld heat treatment. *International Journal of Pressure Vessels and Piping*, 2014, **122**, pp. 6 - 14.

[21] H. Serizawa, S. Nakamura, H. Tanigawa H. Ogiwara H. Murakawa. Numerical study of local pwht condition for eb welded joint between first and side walls in ITER-TBM. *Journal of Nuclear Materials*, 2013, **442(1-3)**, pp. 535 - 540.

[22] Y. Zhang, S. Pratihar, M.E. Fitzpatrick, L. Edwards. Residual stress mapping in welds using the contour method. *Materials Science Forum*, 2004, **490-491**, pp. 294 - 299.

[23] V. Richter-Trummer, S.M.O. Tavares, P.M. G. P. Moreira M.A. V. de Figueiredo, P.M. S. T. de Castro. Residual stress measurement using the contour and the sectioning methods in a mig weld: Effects on the stress intensity factor. *Ciencia & Tecnologia dos Materiais*, 2016, **20(1-2)**, pp. 114 - 119.

[24] M.B. Prime. Cross-sectional mapping of residual stresses by measuring the surface contour after a cut. *Journal of Engineering Materials and Technology*, 2001, **123**, pp. 162 - 168.

[25] *Abaqus Analysis User's Manual, Abaqus 6.12*.

[26] K. Abburi Venkata, C.E. Truman, D.J. Smith, A.K. Bhaduri. Characterising electron beam welded dissimilar metal joints to study residual stress relaxation from specimen extraction. *International Journal of Pressure Vessels and Piping*, 2016, **139-140**, pp. 237 - 249.

[27] K. Abburi Venkata, C.E. Truman, H.E. Coules, A.D. Warren. Applying electron backscattering diffraction to macroscopic residualstress characterisation in a dissimilar weld. *Journal of Materials Processing Technology*, 2017, **241**, pp. 54 - 63.

[28] Asme boiler and pressure vessel code, sections *I*, *II*, and *IX*, and *B*31.1.

[29] K. Abburi Venkata. *Characterising High Energy Beam Welding in Structural Steels with Numerical Simulation and Validation*. PhD thesis, University of Bristol, UK, 2015.

[30] A.H. Yaghi, T.H. Hyde, A.A. Becker, W. Sun. Finite element simulation of welding and residual stresses in a p91 steel pipe incorporating solid-state phase transformation and post-weld heat treatment. *Journal of Strain Analysis*, 2008, **43**, pp. 275 - 293.
[31] O. Muransky, C.J. Hamelin, M.C. Smith, P.J. Bendeich, L. Edwards. The effect of plasticity theory on predicted residual stress fields in numerical weld analyses. *Conputational Materials Science*, 2012, **54**, pp. 125 - 134.
[32] D McLean. The physics of high temperature creep in metals. *Reports on Progress in Physics*, 1966 **29(1)**.
[33] A.M. Brown, M.F. Ashby. On the power-law creep equation. *Scripta METALLURGICA*, 1980, **14**, pp. 1297 - 1302.
[34] X. Shan, C.M. Davies, T. Wangsdan N.P. O'Dowd K.M. Nikbin. Thermo-mechanical modelling of a single-bead-on-plate weld using the finite element method. *International Journal of Pressure Vessels and Piping*, 2009, **86**, pp. 110 - 121.
[35] F. Hosseinzadeh, P. Ledgard, P.J. Bouchard. Controlling the cut in contour residual stress measurements of electron beam welded Ti-6Al-4V alloy plates. *Experimental Mechanics*, 2013 **53(5)**, pp. 829 - 839.
[36] M.B. Prime, R.J. Sebring, J.M. Edwards, D.J. Hughes, P.J. Webster. Laser surface-contouring and spline data-smoothing for residual stress measurement. *Experimental Mechanics*, 2004 **44(2)**, pp. 176 - 184.
[37] M.B. Toparli, M.E. Fitzpatrick, S. Gungor. Improvement of the contour method for measurement of near-surface residual stresses from laser peening. *Experimental Mechanics*, 2013 **53(9)**, pp. 1705 - 1718.
[38] M.D. Olson, T.A. DeWald, M.B. Prime M.R. Hill. Estimation of uncertainty for contour method residual stress measurements. *Experimental Mechanics*, 2014, doi: 10.1007/s11340-014-9971-2.